J Therm Anal Calorim (2010) 102:615–625
DOI 10.1007/s10973-010-0737-5

A simple kinetic method for the determination of the reaction model from non-isothermal experiments

Jordi Farjas · Núria Butchosa · Pere Roura

NATAS2009 Special Issue

Abstract In a recent article, we obtained an approximate solution for the evolution of a transformed fraction under isochronal conditions for a large variety of single-step transformations. We verified that this solution is accurate and can, in many instances, be used instead of the exact numerical solutions of the corresponding differential equations. In this article we want to examine the possibilities offered by an analytical solution in the analysis of thermoanalytical curves. We will show that for single-step transformations, our model predicts that under the proper time scaling the thermograms obtained at different heating rates merge into a single curve. This 'universal curve' is exclusively related to the kinetic model. In addition, the universal curve can be obtained from experimental thermograms by means of a simple transformation. In this way, the dependence of the experimental curves on the rate constant and the kinetic model can easily be separated, making it possible to independently determine the kinetic parameters and the kinetic model. In addition, one can easily check the validity of the kinetic analysis as well as calculate a reliable statistical measure of the goodness of the single-step assumption.

Keywords Solid state reaction · Single-step transformation · Kinetic analysis · Kissinger method · Analytical chemistry

J. Farjas (✉) · N. Butchosa · P. Roura
GRMT, Department of Physics, University of Girona,
Campus Montilivi, Edif. PII, 17071 Girona, Catalonia, Spain
e-mail: jordi.farjas@udg.cat

Introduction

Solid state transformations are usually governed by a single limiting step [1]. In such cases, the evolution over time of the conversion degree, α, is described by a differential equation of the form [2]:

$$\frac{d\alpha}{dt} = k(T)f(\alpha) \tag{1}$$

where t is time, T is the temperature, $k(T)$ is the rate constant and $f(\alpha)$ is the conversion function of a particular reaction model. In most practical situations [3–5], it is possible to assume an Arrhenius temperature dependence for the rate constant:

$$k(T) = A\exp\left(-\frac{E}{RT}\right) \tag{2}$$

where A is constant (the pre-exponential term), E activation energy, and R gas constant. The objective of a kinetic method is the determination of the so-called 'kinetic triplet': A, E, and $f(\alpha)$.

Under isothermal conditions $k(T)$ is constant and the solution of the single-step kinetic equation can be obtained by the direct integration of Eq. 1:

$$g(\alpha) \equiv \int_0^{\alpha} \frac{du}{f(u)} = k(T)(t - t_0) \tag{3}$$

whence

$$\alpha(t) = G(k(T)(t - t_0)) \tag{4}$$

where G is the inverse function of $g(\alpha)$. In ref. [6] the analytical expression for both g and G is given for a number of reaction models, i.e., in most cases one can easily derive an analytical solution under isothermal

conditions. It is worth noting that the thermoanalytical curves obtained at different temperatures differ only by a time scale factor of $\tau \equiv 1/k(T)$.

When the temperature varies with time, Eq. 1 still holds for spatially homogeneous reactions, whereas for heterogeneous reactions, such as crystallization, it is only approximate [7]. The most common non-isothermal experiments are those that are isochronal, i.e., $\beta \equiv dT/dt$ = constant.

We have recently developed [6] an approximate analytical solution of Eq. 1 under isochronal conditions,

$$\alpha(t) = G(z),\ z \equiv g(\alpha_P^\infty)\exp\left(\frac{1}{g(\alpha_P^\infty)}\frac{t}{\tau_P}\right)$$
$$\frac{d\alpha(t)}{dt} = \frac{z}{g(\alpha_P^\infty)\tau_P}\frac{dG}{dz} \quad (5)$$

where T_P is the peak temperature (the temperature at which the transformation rate is at its maximum (see Fig. 1)), $\tau_P \equiv 1/k(T_P)$ and α_P^∞ is $\alpha(T_P)$ for $E/R\ T_P \to \infty$ (the value of α_P^∞ for a number of models is given in the Appendix). The time origin has been shifted so that the maximum transformation rate takes place at $t = 0$; $T = T_P + \beta\ t$. Note that in the definition of $g(\alpha)$, Eq. 3, the initial transformed fraction is zero. Moreover, in the derivation of Eq. 5, it has been assumed that the initial temperature is low enough to neglect the initial transformation rate.

The approximate solution is obtained from the first order series expansion in temperature of $ln[g(\alpha(T))]$ around T_P. The approximate solution is accurate enough provided that the second term in the series expansion is negligible when compared to the first term in an interval of temperatures of the order of the FWHM. As it is stated in the Appendix of ref. [6], the latter condition is equivalent to the validity of the Kissinger relation. Therefore, when the Kissinger relation is accurate, the approximate solution is accurate in the whole temperature range were the transformation takes place. The Kissinger relation is analyzed in the next section.

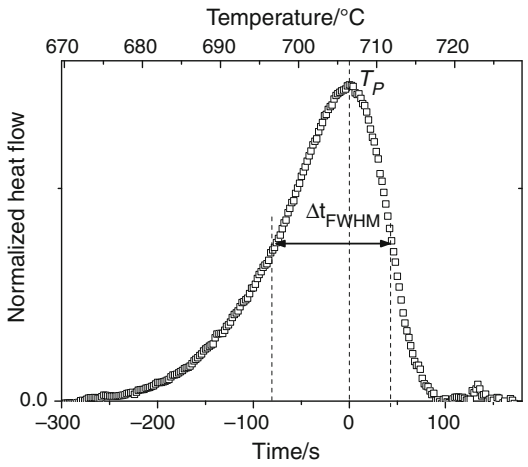

Fig. 1 Determination of the peak temperature, T_P, and full width at half maximum, Δt_{FWHM}, in a DSC thermogram corresponding to the crystallization of amorphous silicon when heated at a constant rate of 8 K/min

Two special features of our approximate solution that account for its simplicity are:

(i) its similarity with the isothermal solution. From Eqs. 4 and 5 one can observe that the only difference between the two solutions is the argument of function G.

(ii) the dependence on the heating rate β and the rate constant $k(T)$ being implicit through the constant τ_P. This means that for a given process all the solutions are identical except for the time constant τ_P.

As with the isothermal case, according to Eq. 5 all the curves obtained at different heating rates differ only by a time scale factor of τ_P. Therefore, when time is normalized by a scale factor τ_P, the evolutions obtained at different heating rates merge into one single curve. Moreover, the shape of this curve does not depend on the rate constant, but is exclusively related to the reaction model $f(\alpha)$.

The significance for both experimental and theoretical purposes of a simple analytical solution is evident. As an example, we have applied it to the analysis of structural relaxation in amorphous materials [8]. In this article, we want to explore the possibilities an approximate analytical solution offers for the analysis of thermoanalytical curves. First, we will discuss how the widely used Kissinger method can be complemented to improve its reliability. Then, we will develop a new method that determines, in a simple and reliable way, the kinetic model that governs the transformation. Finally, we will apply our method to analyze the calorimetric data of the crystallization of amorphous silicon and the thermogravimetric data of $CaCO_3$ decomposition.

Kinetic method

The Kissinger method

Despite the recent development of a wide variety of advanced computational methods for the kinetic analysis of thermoanalytical experiments [9], the Kissinger method is still widely used in the analysis of structural transformations as diverse as the dehydrogenation of carbon nanotubes [10], the crystallization of glasses [11, 12] and the thermal analysis of lipids, proteins and biological membranes [13]. The Kissinger method relies on the approximate relationship [7, 14]:

$$\ln\frac{\beta}{T_P^2} = -\frac{E}{RT_P} + \ln\frac{AR}{E} + \ln\left(-\left.\frac{\mathrm{d}f(\alpha)}{\mathrm{d}\alpha}\right|_{\alpha=\alpha_P^\infty}\right) \quad (6)$$

In the derivation of Eq. 6 it has been assumed that $\alpha_P \simeq \alpha_P^\infty$. For many reaction models $\mathrm{d}f(\alpha)/\mathrm{d}\alpha|_{\alpha=\alpha_P^\infty} = -1$ [6, 14]. In this case, Eq. 6 is reduced to the relation originally derived by Kissinger for a first order reaction [15].

The main advantages of the Kissinger method are its simplicity and accuracy. For a series of experiments performed at different heating rates the slope of $\ln \beta/T_P^2$ vs. $1/T_P$ (the Kissinger plot) is just the activation energy. The method is also very accurate for single-step processes provided that $E/R\ T_P$ is large enough (typically $E/R\ T_P \geq 10$ [16]). A literature review confirms that this last consideration does not represent a serious limitation. For instance, $E/R\ T_P > 25$ for most glass-crystal transformations [17], and we have found values in the 8–35 range for reactions involving polymers [18] and thermal decomposition of molecules [10, 19] (among these, values below 10 are scarce). Moreover, as Starink [20] pointed out, 'the overwhelming majority of reactions occur for $15 < E/R\ T_P < 60$'.

A noteworthy property of the Kissinger method is that the determination of the activation energy does not depend on the particular mechanism that governs the transformation. Its main drawback is that, even in the case of complex mechanisms or for transformations involving more than one step, one can obtain a good fitting from which an empirical activation energy of doubtful meaning can be deduced. Consequently, from the Kissinger plot one cannot conclude whether the transformation follows a single-step or a more complex process [21]. This fact makes it necessary to perform additional tests to validate the kinetic analysis. On the other hand, the peak width (see Fig. 1) is a parameter that is very sensitive to the occurrence of multiple transformations. According to Eq. 5, the full width at half maximum (FWHM) is proportional to τ_P,

$$\Delta t_{\mathrm{FWHM}} = \Delta t'_{\mathrm{FWHM}} \cdot \tau_P \quad (7)$$

where $\Delta t'_{\mathrm{FWHM}}$ is the FWHM of the curve obtained when time is normalized to $\tau_P = 1$, i.e., is a constant that depends exclusively on the particular kinetic model (in the Appendix we describe how $\Delta t'_{\mathrm{FWHM}}$ can be calculated and its value is given for a number of reaction models). If we substitute the definition of τ_P into the previous expression we obtain a relation similar to the Kissinger equation (Eq. 6):

$$\ln(\Delta t_{\mathrm{FWHM}}) = \frac{E}{RT_P} + \ln\frac{\Delta t'_{\mathrm{FWHM}}}{A} \quad (8)$$

In fact, the value of the slope coincides with the absolute value of the slope of the Kissinger plot. Since the peak width is sensitive to deviations from single-step kinetics, the combined plots of $ln\ \beta/T_P^2$ and $\ln(\Delta t_{\mathrm{FWHM}})$ vs. $1/T_P$ provide a more reliable determination of the activation energy.

The isochronal universal curve

As indicated in the introduction, according to our approximate analytical solution, for a given reaction model all the transformation rate curves measured at different heating rates merge into one single curve when time is properly scaled. This single curve depends exclusively on the reaction model, i.e., it is independent of the rate constant. We will refer to this curve as the 'universal curve'. In this section, we will obtain the universal curve and develop a simple approach to match the experimental data to this curve. The advantage of this approach is clear: it allows a direct determination of the reaction model. It is worth noting that this method complements the Kissinger and isoconversional methods that allow the transformation rate to be determined independently of the particular reaction model, with the result that one can separate the contributions of the transformation rate and the reaction model.

According to our model, a universal curve is obtained when the time is scaled with the proper time scale factor. In terms of specific time scale factors one can use Δt_{FWHM}, a parameter that is easily determined from the experimental curves. Moreover, Δt_{FWHM} is proportional to τ_P (see Eq. 7) so that when time is scaled by Δt_{FWHM} in Eq. 5, the dependence on τ_P disappears and we obtain a curve that depends exclusively on the reaction model,

$$\begin{aligned} &\alpha(t') = G(z'),\ z' \equiv g(\alpha_P^\infty)\exp\left(\frac{\Delta t'_{\mathrm{FWHM}}}{g(\alpha_P^\infty)}t'\right) \\ &\frac{\mathrm{d}\alpha(t')}{\mathrm{d}t'} = \frac{\Delta t'_{\mathrm{FWHM}}}{g(\alpha_P^\infty)}z'\frac{\mathrm{d}G(z')}{\mathrm{d}z'} \end{aligned} \quad (9)$$

where $t' \equiv t/\Delta t_{\mathrm{FWHM}}$ is the scaled time. As expected, the universal curve, Eq. 9, depends exclusively on the kinetic model, as the dependence on the rate constant has disapeared. In Figs. 2 and 3 we have plotted the universal curve for a number of models, whose g and G functions, and the values of $\Delta t'_{\mathrm{FWHM}}$ and $g(\alpha_P^\infty)$ are given in the Appendix. Given the large number of models, we have split the curves into two sets, in both of which the first order model is plotted as a reference. Some universal curves are identical, viz.:

(i) the first-order reaction and KJMA model of any Avrami exponent n, Eq. 10,
(ii) one-dimensional diffusion, the power law for any exponent n and the zero order reaction

On the other hand, the n-dimensional reaction and the n-order reaction models are mathematically identical when the exponent is properly transformed.

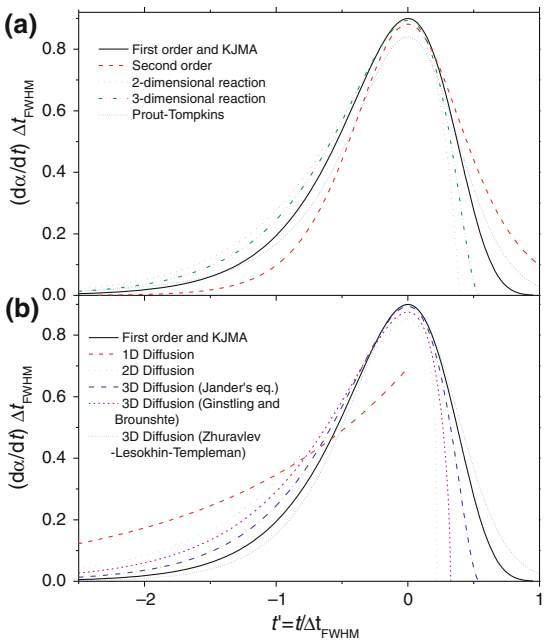

Fig. 2 Universal curve, Eq. 9, for the evolution of the transformation rate, $d\alpha/dt$. The approximate solution of these models is given in the Appendix. The initial transformed fraction for all the curves is 0 except for the Prout–Tompkins which is 0.01

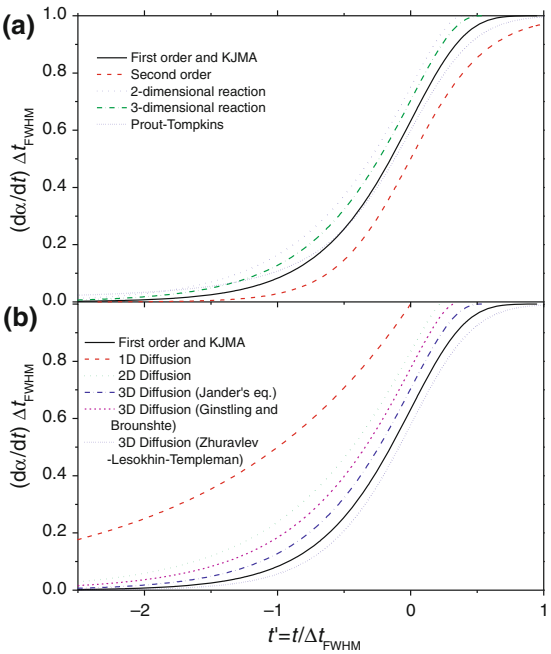

Fig. 3 Universal curve, Eq. 9, for the evolution of the transformed fraction α. The approximate solution of these models is given in the Appendix. The initial transformed fraction for all the curves is 0 except for the Prout–Tompkins which is 0.01

Figures 2 and 3 show clearly that isochronal experiments are less sensitive to the reaction model than isothermal ones (see Fig. 1 in Ref. [22]). From Eqs. 4 and 5 one can verify that the only difference between isothermal and the isochronal solutions is the argument of the function $G(z)$. This argument is proportional to time for the isothermal solution but has an exponential dependence on time in the isochronal case. This exponential dependence on time is responsible for the loss of sensitivity, which is therefore intrinsic to the experiments performed at a constant heating rate. For non-isothermal measurements, the sensitivity to the reaction model can be improved by means of controlled rate thermal analysis [23], in which the rate of the sample property changes is controlled by controlling the sample temperature. However, the use of controlled rate thermal analysis is quite limited due the lack of commercial equipment prepared to perform this kind of measurements.

Besides, to determine the reaction model the experimental thermograms are also to be scaled. The corresponding transformations are:

(i) the thermograms are to be normalized to obtain either the transformed fraction α or the transformation rate $d\alpha/dt$,
(ii) the time origin is to be placed at the peak temperature, and
(iii) the time is to be divided by the curve's Δt_{FWHM} to obtain the scaled time t'.

Then, direct comparison between the universal curves and the scaled thermograms allows determination of the reaction model.

To illustrate our approach, we will apply it to the numerical simulation of the crystallization of a-Si. The crystallization of a-Si can be properly described [24–26] by the Kolmogorov–Johnson–Mehl–Avrami (KJMA) model [7, 27–31]:

$$f(\alpha) = n(1-\alpha)[-\ln(1-\alpha)]^{\frac{n-1}{n}}. \tag{10}$$

In Fig. 4, we have plotted the related time-scaled curves. These curves have been calculated from the numerical integration of Eq. 1 under isochronal conditions and for different values of the heating rate. One can verify that the time-scaled evolutions obtained at different heating rates merge into one single curve as predicted by our approximate solution.

In addition, in Fig. 4 we have plotted the universal curve (solid line). The universal curve for the KJMA is obtained from Eq. 9 after substituting the corresponding G function and the values of the constants $\Delta t'_{FWHM}$ and $g(\alpha_P^{\infty})$ (see the Appendix):

$$\alpha(t') = 1 - \exp[-\exp(2.44639t')]$$
$$\frac{d\alpha(t')}{dt'} = 2.44639\exp[-\exp(2.44639t')]\exp(2.44639t') \tag{11}$$

It is worth noting that the plot of the universal curve is not a fit. In fact, there is only one single universal curve

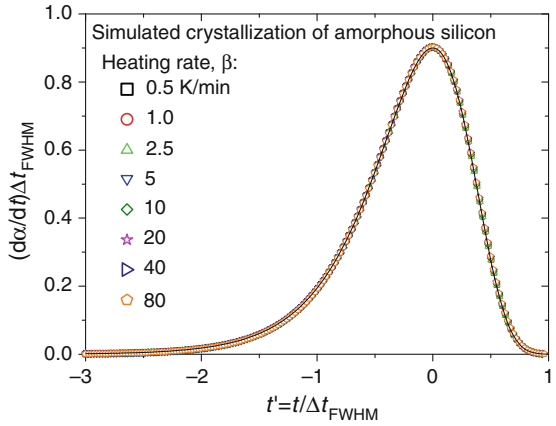

Fig. 4 Symbols are the time-scaled curves of the simulated a-Si crystallization obtained at different heating rates and the solid line is the theoretical KJMA universal curve, Eq. 11. The kinetic parameters of the simulation are E = 352.155KJ/mol and $A = 3.11\ 10^{16}$ 1/s, and the reaction model is the KJMA model with $n = 4$

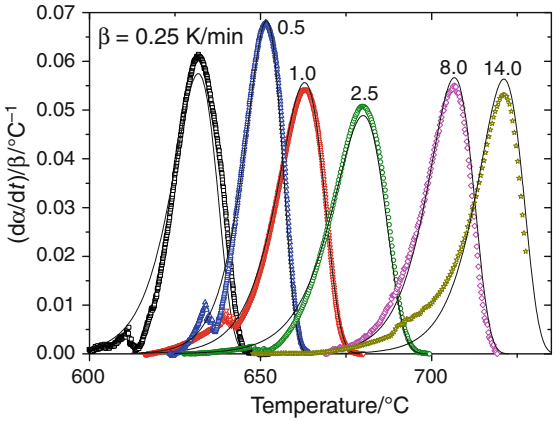

Fig. 5 Symbols are DSC thermograms of a-Si crystallization and solid lines are the predicted curves obtained from the KJMA theoretical universal curve

related to the KJMA model. It is also remarkable the coincidence in Fig. 4 between the scaled curves derived from the exact solution of Eqs. 1 and 10, and the universal curve derived from the approximate solution, Eq. 5. In addition, this nice agreement shows that the approximate solution is accurate in the whole temperature interval were the the reaction takes place. In ref. [32], we have tested the accuracy of the approximate solution for the KJMA model.

In the two following sections, we will apply our kinetic method to two different sets of experimental curves: the crystallization of a-Si by DSC and the thermal decomposition of $CaCO_3$ by thermogravimetry.

Crystallization of amorphous silicon

a-Si films were prepared by plasma-enhanced chemical vapor deposition (PECVD) [25] with a thickness of around 10μm. Calorimetric measurements were carried out in a Mettler Toledo differential scanning calorimeter (DSC), model 822. Experiments were performed by heating the sample at several heating rates in an inert atmosphere of Ar. DSC thermograms (Fig. 5) were obtained by subtracting the curves of the second and first heating measurements and dividing the DSC signal by the total area under the curve to obtain the transformation rate.

The related Kissinger and $\ln(\Delta t_{FWHM})$ plots are shown in Fig. 6. The activation energies obtained from the Kissinger and $\ln(\Delta t_{FWHM})$ plots are 346 and 343 KJ/mol, respectively. The agreement between the two results confirms that the crystallization of a-Si is approximately described by a single-step process. Moreover, these values of the activation energy are in good agreement with the expected value for homogeneous nucleation and three-dimensional growth, 352 KJ/mol [24, 25], so the reaction model should approximately coincide with the KJMA model.

To confirm this expectation, we have plotted the scaled thermograms together with the KJMA universal curve, Eq. 11, as shown in Fig. 7.

From Fig. 7 one can see that crystallization of a-Si is in agreement with the KJMA model. This agreement is more apparent from the comparison between the universal curve and the curve obtained after averaging the scaled thermograms (see Fig. 7.b). It is worth recalling that the solid line (universal curve) in Fig. 7 is not a fitting.

Once the reaction model has been established, one can easily reproduce the evolution of the transformed fraction for a given heating rate. This evolution is given by the approximate solution Eq. 5 by simply reversing the time-scaling transformation used in the derivation of the universal curve. Figure 5 establishes that the agreement

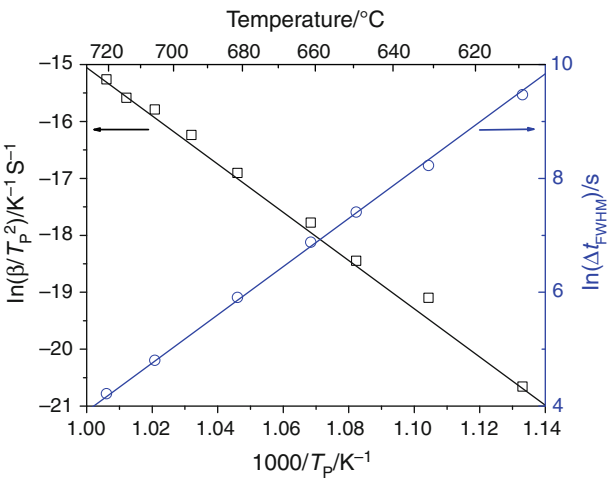

Fig. 6 Kissinger and $\ln(\Delta t_{FWHM})$ plots for the crystallization of a-Si corresponding to DSC thermograms plotted in Fig. 5

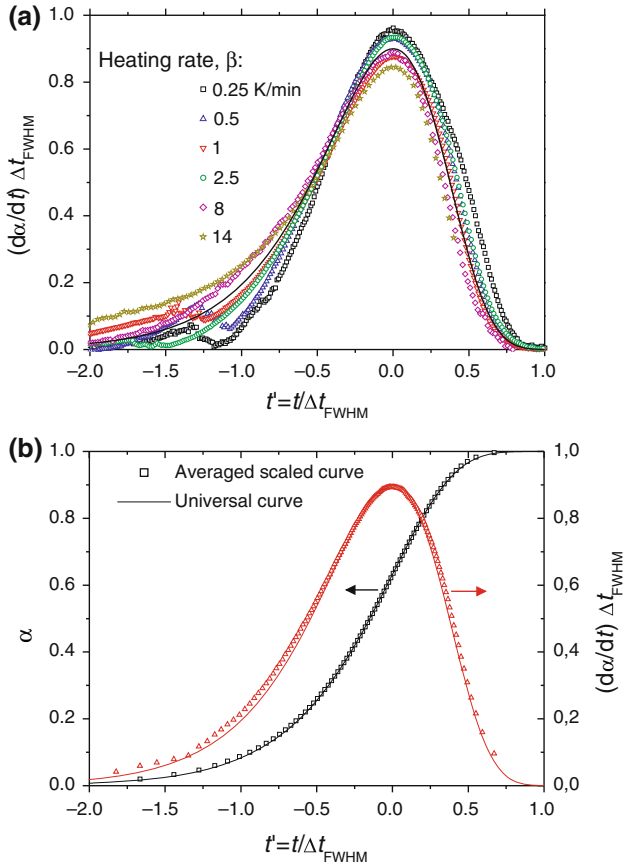

Fig. 7 **a** Symbols are the time-scaled curves of the thermograms plotted in (Fig. 5), and the solid line is the theoretical KJMA universal curve, Eq. 11. **b** Symbols are the averaged scaled curve, and the solid line is the theoretical KJMA universal curve, Eq. 11

between the experimental data and the predicted evolution is remarkable. However, a clear deviation from the theoretical model at the beginning of the transformation is also apparent. This discrepancy and notably, the appearance of a weak sharp pre-peak, is related to the heterogeneous nucleation on the film surface. Since the films are quite thick (10μm), the observed behavior corresponds mainly to homogeneous nucleation and growth, although a minor contribution from the faster heterogeneous nucleation is detectable on the low temperature side.

Thermal decomposition of $CaCO_3$

High purity $CaCO_3$ powders were provided by Panreac Quimica S.A.U. Thermal decomposition of these powders has been carried out in a Mettler Toledo thermogravimeter, model TGA851LF. The powders were placed in platinum crucibles and experiments were performed by heating the sample at several heating rates while keeping a high purity N_2 gas flow rate.

The thermal decomposition of $CaCO_3$ behaves as a single-step reaction provided that the reverse reaction is prevented [33]. This condition is achieved by maintaining a very low carbon dioxide partial pressure, $P(CO_2)$. We performed two sets of experiments with different N_2 gas flow rates: 40 and 300 mL/min. The higher the N_2 gas flow, the lower the $P(CO_2)$. In Fig. 8 we have plotted the time derivative of the mass normalized to the total mass change (transformation rate) for the two sets of measurements.

To confirm that the reaction behaves as a single-step transformation, we performed the corresponding Kissinger and $\ln(\Delta t_{FWHM})$ plots (see Fig. 9). The results of the linear fitting are summarized in Table 1. From the linear correlation coefficient, r^2, it can be seen that the goodness of the fits is nearly the same. However, there is a perceptible difference between the activation energies obtained from the Kissinger and width analysis: the experiments performed at a higher N_2 flow rate exhibit the best agreement. This result is consistent with the fact that the experiments performed at a lower $P(CO_2)$ are expected to have a lower contribution of the reverse reaction. It is clear, therefore, that the assumption of single-step kinetics can not rely exclusively on the goodness of the Kissinger fit.

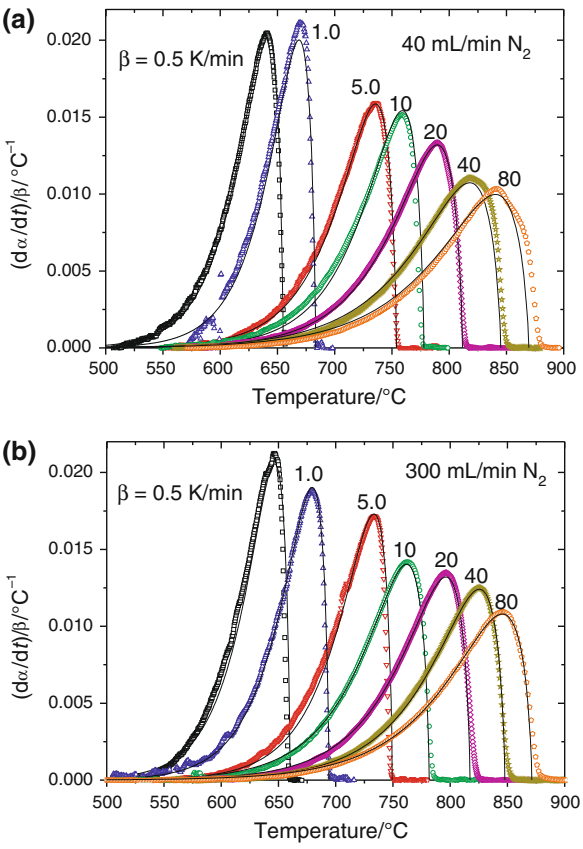

Fig. 8 Symbols are the evolution of the decomposition rate of $CaCO_3$ for two different N_2 flow rates and solid lines are the predicted curves obtained from the Fn theoretical universal curve Eq. 13

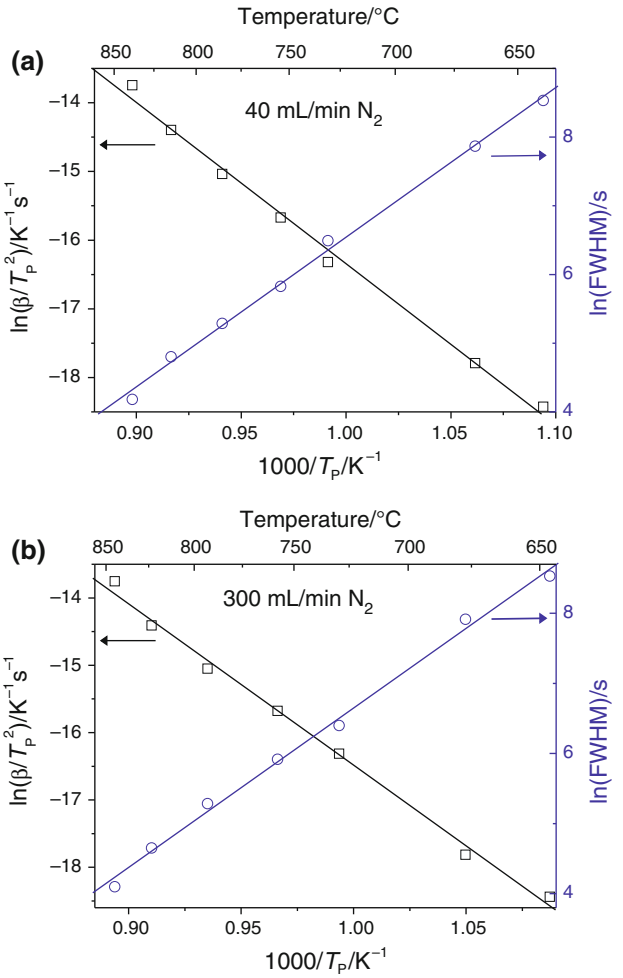

Fig. 9 Kissinger and $\ln(\Delta t_{\mathrm{FWHM}})$ plots for the decomposition rate of $CaCO_3$ corresponding to the evolutions plotted in Fig. 8

Table 1 Results of the linear fittings shown in Fig. 9

	40/mL min^{-1}		300/mL min^{-1}	
	E/KJ mol^{-1}	r^2	E/KJ mol^{-1}	r^2
Kissinger	195.2	0.997	199.3	0.997
FWHM	181.0	0.998	189.1	0.998
Difference	14.2		10.2	

Conversely, the combined analysis of the Kissinger and $\ln(\Delta t_{\mathrm{FWHM}})$ plots is useful for checking this assumption.

To confirm the latter conclusion, we have calculated the activation energy by means of Vyazovkin's advanced isoconversional method [34]. The result is plotted in Fig. 10. One can observe that in both cases we obtain a relative constant value of the activation energy. It is also clear that the smoothest variation of the activation energy is the one related to the highest N_2 flow rate. This result confirms that the measurements performed at the lowest $P(CO_2)$ are the ones that best agree with a single-step kinetics model.

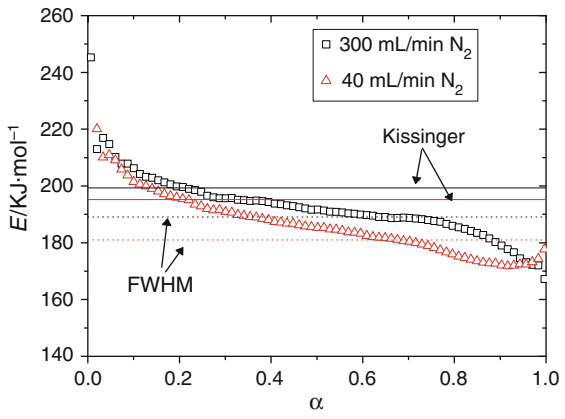

Fig. 10 Activation energies for the thermal decomposition of $CaCO_3$ related to the thermograms plotted in Fig. 8. The activation energies have been calculated using the Vyazovkin's advanced isoconversional method [34]

In Fig. 11 we have plotted the scaled thermograms of Fig. 8. In both cases there is a nice superposition of the scaled curves which confirms the single-step kinetics behavior. To establish the reaction model, we fitted the scaled curves to the corresponding universal curve. The shape of the scaled curves agrees with the universal curve of the nth-order rate reaction, Fn (and the equivalent n-dimensional reaction, Rn). This conclusion coincides with results reported by other authors [9, 35–37]. The nth-order rate reaction model is given by

$$f(\alpha) = (1-\alpha)^n, \tag{12}$$

and the corresponding universal curve is (see the Appendix),

$$\begin{aligned} \alpha(t') &= 1 - \left[1 + (n-1)\exp(\Delta t'_{\mathrm{FWHM}} \cdot t')\right]^{\frac{1}{1-n}} \\ \frac{\mathrm{d}\alpha(t')}{\mathrm{d}t'} &= \Delta t'_{\mathrm{FWHM}} \left[1 + (n-1)\exp(\Delta t'_{\mathrm{FWHM}} \cdot t')\right]^{\frac{n}{1-n}} \\ &\quad \times \exp(\Delta t'_{\mathrm{FWHM}} \cdot t') \end{aligned} \tag{13}$$

For the Fn model, there is not an analytical relation between $\Delta t'_{\mathrm{FWHM}}$ and n. We have included an approximate relation between $\Delta t'_{\mathrm{FWHM}}$ and n in the Appendix.

The best fit to the universal curve corresponds to an exponent $n = 0.42$ and $n = 0.40$ for the measurements carried out at an N_2 gas flow rate of 40 and 300 mL/min, respectively. The related universal curves are represented as a solid line in Fig. 11. In Fig. 12 we have plotted the average of the scaled curves of Fig. 11 and the fitted universal curve. From Figs. 11 and 12 it is clear that the agreement between the scaled thermograms and the fitted universal curve is remarkable. Similarly to the previous case, once the universal curve has been determined it is possible to predict the evolution for a given heating rate. This evolution is given by the approximate solution, Eq. 5, and is plotted in Fig. 8 together with the measured

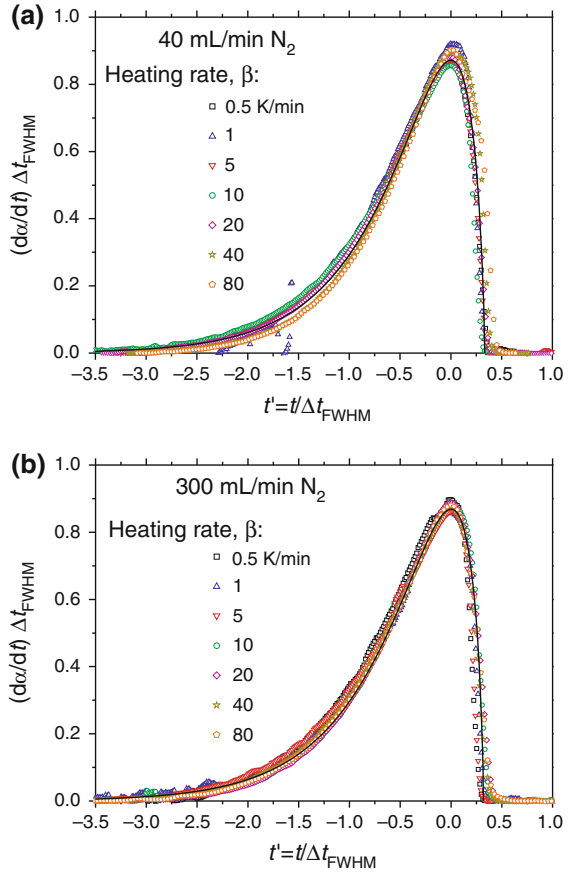

Fig. 11 Symbols are the time-scaled curves of the thermograms plotted in Fig. 8, and the solid line is the fitted theoretical *n*-order reaction universal curve Eq. 13, with $n = 0.42$ (**a**) and $n = 0.40$ (**b**)

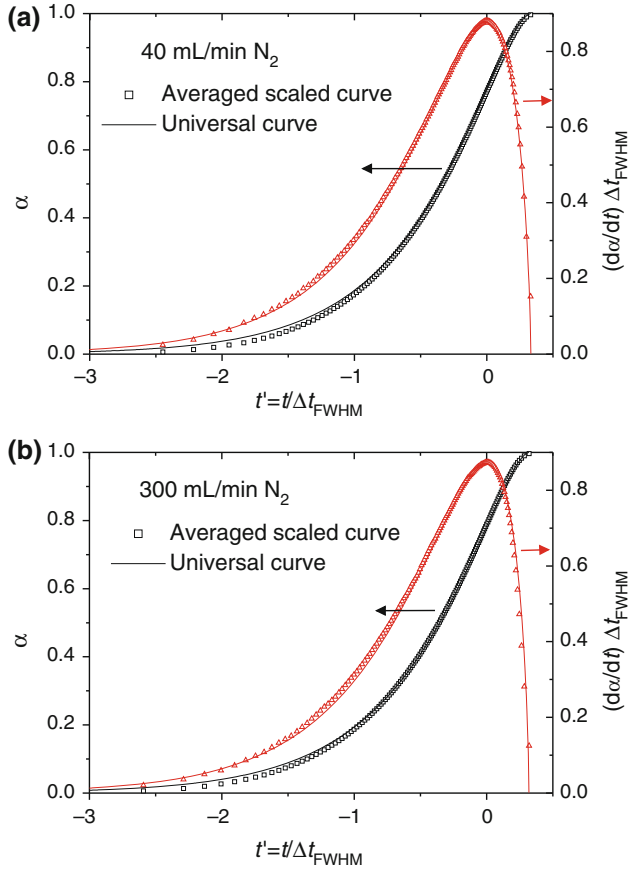

Fig. 12 Symbols are the average of the scaled curves plotted in Fig. 11, and the solid line is the fitted theoretical *n*-order reaction universal curve, Eq. 13, with $n = 0.42$ (**a**) and $n = 0.40$ (**b**)

evolution of the transformation rate. As expected, there is good agreement between the predicted and the actual evolutions. However, one can discern deviations between the actual and predicted evolutions for the lowest N_2 flow rate and at the highest heating rate. In fact, the higher the heating rate the higher the CO_2 emission rate, so the most favorable conditions for the occurrence of a reverse reaction are a low N_2 flow rate and a high heating rate. These small deviations from single-step kinetics account for the discrepancies observed in the combined analysis of Kissinger and width plots (see Table 1).

It is worth noting that a fine overlap of the scaled thermograms guarantees that the reaction can be accurately described by single-step kinetics in the temperature range analyzed. Actually, one can obtain a statistical parameter measuring the goodness of the single-step approximation from the deviations of the scaled thermograms from their averaged curve. For instance, the average standard deviations are 0.07 and 0.05 for the measurements performed at a N_2 gas flow rate of 40 and 300 mL/min, respectively. Therefore, as expected, the lower the $P(CO_2)$, the better the single-step approximation. Besides, from the deviations of the scaled thermograms from the universal curve, one can derive a statistical quantitative measure for the goodness of the reaction model fitting.

Conclusions

We have proved that isochronal experiments are less sensitive to the reaction model than isothermal ones.

The combined analysis of the Kissinger and $\ln(\Delta t_{FWHM})$ plots, a generalized Kissinger plot, is a simple and accurate method to determine the activation energy and its reliability. In addition, it allows us to check whether or not the reaction is approximately governed by a single limiting step in the temperature range analyzed.

Furthermore, the analysis of the universal curve allows the reaction model to be easily determined by removing the contribution of the rate constant. This method complements the isoconversional and generalized Kissinger plot methods, which allow the activation energy to be determined independently of the reaction model.

Moreover, a good overlap of the scaled thermograms ensures that the observed evolution of the transformation can be described by single-step kinetics in the temperature range studied. The deviation of the scaled thermograms from their averaged curve indicates the goodness of the single-step approximation.

To sum up, we believe that our kinetic method makes the analysis of isochronal data as simple as the analysis of isothermal data.

Acknowledgements This study was partially funded by the Spanish Programa Nacional de Materiales under contract No. MAT2009-08385 and by the Generalitat de Catalunya contract No. 2009SGR-185.

Appendix

Parameters of the universal curve

To derive the universal curve, Eq. 9, for a given reaction model one needs to know the functions g and G, and the constants $g(\alpha_P^\infty)$ and $\Delta t'_{\mathrm{FWHM}}$.

Function $g(\alpha)$ is defined in Eq. 3 and is the integral from zero to a given transformed fraction α of the reciprocal of the conversion function f.

G is the inverse function of $g(\alpha)$:

$$\alpha = G(z) \Leftrightarrow g(\alpha) = z \tag{14}$$

α_P^∞ is $\alpha(T_P)$ for $E/R\ T_P \to \infty$. α_P^∞ is given by the relationship [38, 39]:

$$f'(\alpha_P^\infty) g(\alpha_P^\infty) = -1 \tag{15}$$

Finally, $\Delta t'_{\mathrm{FWHM}}$ is the FWHM of the conversion rate peak when τ_P is replaced by a factor 1. The maximum transformation rate takes place at $t = 0$, and has the value, Eq. 5,

$$\left.\frac{\mathrm{d}\alpha}{\mathrm{d}t}\right|_{\max} = \left.\frac{\mathrm{d}G}{\mathrm{d}z}\right|_{z=g(\alpha_P^\infty)} \tag{16}$$

Then, the equation:

$$\frac{z}{g(\alpha_P^\infty)}\frac{\mathrm{d}G}{\mathrm{d}z} = \frac{1}{2}\left.\frac{\mathrm{d}G}{\mathrm{d}z}\right|_{z=g(\alpha_P^\infty)} \tag{17}$$

has two solutions and $\Delta t'_{\mathrm{FWHM}}$ is the difference between the time instants given by these two solutions. In the following we include the functions g and G, and the constants $g(\alpha_P^\infty)$ and $\Delta t'_{\mathrm{FWHM}}$, for several reaction models.

The KJMA model

The conversion function for the KJMA model is

$$f(\alpha) = n(1-\alpha)[-\ln(1-\alpha)]^{\frac{n-1}{n}}. \tag{18}$$

Then,

$$g(\alpha) = [-\ln(1-\alpha)]^{1/n}, \tag{19}$$

$$G(z) = 1 - \exp[-z^n], \tag{20}$$

$\alpha_P^\infty = 1 - e^{-1}, g(\alpha_P^\infty) = 1$ and $\Delta t'_{\mathrm{FWHM}} = 2.44639/n$. Both G and $\Delta t'_{\mathrm{FWHM}}$ depend on the exponent n. However, when G and $\Delta t'_{\mathrm{FWHM}}$ are substituted into Eq. 9, this dependency on n disappears. Therefore, there is one single universal curve for the KJMA model, Eq. 11.

The nth-order rate reaction model

The conversion function for the F(n) model is

$$f(\alpha) = (1-\alpha)^n. \tag{21}$$

Then,

$$g(\alpha) = \frac{(1-\alpha)^{1-n} - 1}{n-1}, \tag{22}$$

$$G(z) = 1 - [1 + (n-1)z]^{1/(1-n)}, \tag{23}$$

$\alpha_P^\infty = 1 - n^{1/(1-n)}$ and $g(\alpha_P^\infty) = 1$. Unfortunately, there is no analytical solution for $\Delta t'_{\mathrm{FWHM}}$. We have fitted the the evolution of $\Delta t'_{\mathrm{FWHM}}$ with n to two polynomials of order three:

$$\begin{aligned}\Delta t'_{\mathrm{FWHM}} &= 0.734522 + 2.76478n - 1.75728n^2 \\ &\quad + 0.714863n^3, \quad n \le 1 \\ \Delta t'_{\mathrm{FWHM}} &= 1.41394 + 1.13486n - 0.0481617n^2 \\ &\quad + 0.00211241n^3, \ 1 < n < 10\end{aligned} \tag{24}$$

The absolute error of this fit is less than 0.05.

Finally, Eqs. 22 and 23 fail for the first ordre reaction, $n = 1$. However, this particular case is mathematically identical to the KJMA model with $n = 1$.

The nth-dimensional reaction model

The conversion function for the R(n) model is

$$f(\alpha) = (1-\alpha)^{(n-1)/n}. \tag{25}$$

The R(n) model is mathematically identical to the F(n') model with $n' = (n-1)/n$.

The power law reaction model

The conversion function for the P(n) model is

$$f(\alpha) = n\alpha^{(n-1)/n}. \tag{26}$$

Then,

$$g(\alpha) = \alpha^{1/n}, \tag{27}$$

$$G(z) = z^n, \tag{28}$$

$\alpha_P^\infty = 1, g(\alpha_P^\infty) = 1$ and $\Delta t'_{\mathrm{FWHM}} = \ln(2)/n$. Like the KJMA model, in Eq. 9 the dependency on n disappears. Therefore, there is one single universal curve for the P(n) model. This universal curve is identical to the zeroth-order reaction model, F(0).

The 1D diffusion

The conversion function for the D1 model is

$$f(\alpha) = (2\alpha)^{-1}. \tag{29}$$

Then,

$$g(\alpha) = \alpha^2, \tag{30}$$

$$G(z) = \sqrt{z}, \tag{31}$$

Then,

$$g(\alpha) = \left[1 - (1-\alpha)^{1/3}\right]^2, \tag{36}$$

$$G(z) = -3z + (3+z)\sqrt{z}, \tag{37}$$

$\alpha_P^\infty = 19/27, g(\alpha_P^\infty) = 1/9$ and $\Delta t'_{\mathrm{FWHM}} = 0.44669$.

The 3D diffusion Ginstling and Brounshte model

The conversion function for the D4 model is

$$f(\alpha) = \frac{3}{2}\left[(1-\alpha)^{-1/3} - 1\right]^{-1}. \tag{38}$$

Then,

$$g(\alpha) = 1 - \frac{2}{3}\alpha - (1-\alpha)^{2/3}, \tag{39}$$

$$G(z) = \frac{3}{8}\left[1 - 4z - 2\sqrt{1+24z}\sin\left(\arctan\left[\frac{8\sqrt{3z(1-3z)^3}}{1-60z-72z^2}\right]/3\right)\right], \tag{40}$$

$\alpha_P^\infty = 1, g(\alpha_P^\infty) = 1$ and $\Delta t'_{\mathrm{FWHM}} = \ln(4)$. The universal curve of the 1D model coincides with the universal curve of the zeroth-order reaction model, F(0).

The 2D diffusion

The conversion function for the D2 model is

$$f(\alpha) = 1/[-\ln(1-\alpha)]. \tag{32}$$

Then,

$$g(\alpha) = (1-\alpha)\ln(1-\alpha) + \alpha, \tag{33}$$

$\alpha_P^\infty = 0.833587, g(\alpha_P^\infty) = 0.53516$ and $\Delta t'_{\mathrm{FWHM}} = 1.5251$. Unfortunately, there is no analytical solution for the inverse function G. However, it can be approximate to,

$$G(z) = 1/2\left(-z + \sqrt{z(8+z)}\right), \tag{34}$$

The absolute error introduced by this approximation is lees than 0.03.

The 3D diffusion Jander's equation

The conversion function for the D3 model is

$$f(\alpha) = \frac{3(1-\alpha)^{2/3}}{2\left[1-(1-\alpha)^{1/3}\right]}. \tag{35}$$

$\alpha_P^\infty = 0.77566, g(\alpha_P^\infty) = 0.113685$ and $\Delta t'_{\mathrm{FWHM}} = 0.376771$.

The 3D diffusion Zhuravlev–Lesokhin–Tempelman equation

The conversion function for the D5 model is

$$f(\alpha) = \frac{3(1-\alpha)^{5/3}}{2\left[1-(1-\alpha)^{1/3}\right]}. \tag{41}$$

Then,

$$g(\alpha) = \frac{\left(1-(1-\alpha)^{1/3}\right)^2}{(1-\alpha)^{2/3}}, \tag{42}$$

$$G(z) = \frac{z(z^2-3z+6) - (3+z)\sqrt{z}}{(z-1)^3}, \tag{43}$$

$\alpha_P^\infty = 37/64, g(\alpha_P^\infty) = 1/9$ and $\Delta t'_{\mathrm{FWHM}} = 0.629728$.

References

1. Brown M, Dollimore D, Galwey A. Comprehensive chemical kinetics. In: Bamford C, Tipper CFH, editors. Reactions in the solid state. vol 22. Amsterdam: Elsevier; 1980. p. 41–113.

2. Henderson DW. Thermal-analysis of nonisothermal crystallization kinetics in glass forming liquids. J Non-Cryst Solids 1979;30:301–15.
3. Raghavan V, Cohen M. Solid-state transformations. In: Hannay N, editor. Treatise of solid state chemistry. vol 5. New York: Plenum Press; 1975. p. 67–127
4. Le Claire A. Diffusion. In: Hannay N, editor. Reactivity of solids. vol 4. New York: Plenum Press; 1975. p. 1–59
5. Vyazovkin S, Wight CA. Isothermal and nonisothermal reaction kinetics in solids: in search of ways toward consensus. J Phys Chem A. 1997;101:8279–84.
6. Farjas J, Roura P. Simple approximate analytical solution for nonisothermal single-step transformations: kinetic analysis. AICHE J. 2008;54:2145–54.
7. Farjas J, Roura P. Modification of the Kolmogorov–Johnson–Mehl–Avrami rate equation for non-isothermal experiments and its analytical solution. Acta Mater. 2006;54:5573–79.
8. Roura P, Farjas J. Structural relaxation kinetics for first- and second-order processes: application to pure amorphous silicon. Acta Mater. 2009;57:2098–107.
9. Brown ME et al. Computational aspects of kinetic analysis. Part A: the ICTAC kinetics project-data, methods and results. Thermochim Acta. 2000;355:125–43.
10. Lee JW, Kim HS, Lee JY, Kang JK. Hydrogen storage and desorption properties of ni-dispersed carbon nanotubes. Appl Phys Lett. 2006;88:143–26.
11. Jóna E, Šimon P, Nemčeková K, Pavlík V, Rudinská G, Rudinská E. Thermal properties of oxide glasses. J Therm Anal Calorim. 2006;84:673–7.
12. Srivastava AP, Srivastava D, Dey GK. A study on microstructure, magnetic properties and kinetics of the nanocrystallization of Fe40Ni38b18m04 metglass. J Magn Magn Mater. 2006;306: 147–55.
13. Ladbrook B, Chapman D. Thermal analysis of lipids, proteins and biological membranes. A review and summary of some recent studies. Chem Phys Lipids. 1969;3:304–56.
14. Mianowski A. The Kissinger law and isokinetic effect. Part I. Most common solutions of thermokinetic equations. J Therm Anal Calorim. 2003;74:953–73.
15. Kissinger HE. Reaction kinetics in differential thermal analysis. Anal Chem. 1957;29:1702–6.
16. Budrugeac P, Segal E. Applicability of the Kissinger equation in thermal analysis revisited. J Therm Anal Calorim. 2007;88: 703–7.
17. Yinnon H, Uhlmann D. Applications of thermoanalytical techniques to the study of crystallization kinetics in glass-forming liquids. Part 1: theory. J Non-Cryst Solids. 1983;54:253–75.
18. Vyazovkin S, Sbirrazzuoli N. Isoconversional kinetic analysis of thermally stimulated processes in polymers. Macromol Rapid Commun. 2006;27:1515–32.
19. Padhi SK. Solid-state kinetics of thermal release of pyridine and morphological study of [ni(ampy)$_2$(no$_3$)$_2$]; ampy=2-picolylamine. Thermochim Acta. 2006;448(1):1–6.
20. Starink MJ. The determination of activation energy from linear heating rate experiments: a comparison of the accuracy of isoconversion methods. Thermochim Acta. 2003;404:163–76.
21. Sbirrazzuoli N, Brunel D, Elegant L. Neural networks for kinetic parameters determination, signal filtering and deconvolution in thermal analysis. J Therm Anal Calorim. 1997;49:1553–64.
22. Vyazovkin S. Kinetic concepts of thermally stimulated reactions in solids: a view from a historical perspective. Int Rev Phys Chem. 2000;19:45–60.
23. Rouquerol J. Controlled transformation rate thermal analysis: the hidden face of thermal analysis. Thermochim Acta. 1989;144: 209–24.
24. Spinella C, Lombardo S, Priolo F. Crystal grain nucleation in amorphous silicon. J Appl Phys. 1998;84:5383–414.
25. Farjas J, Rath C, Roura P, Roca i Cabarrocas P. Crystallization kinetics of hydrogenated amorphous silicon thick films grown by plasma-enhanced chemical vapour deposition. Appl Surf Sci. 2004;238:165–8.
26. Farjas J, Roura P, Rocai Cabarrocas P. Grain size control by means of solid phase crystallization of amorphous silicon. In: Chu V, Miyazaki S, Nathan A, Yang J, Zan H, editors. Amorphous and polycrystalline thin-film silicon science and technology. vol 989. Warrendale: Mater Res Soc; 2007. p. 139–44.
27. Avrami M. Kinetics of phase change. I general theory. J Chem Phys. 1939;7:1103–12.
28. Avrami M. Kinetics of phase change. II transformation-time relations for random distribution of nuclei. J Chem Phys. 1940;8:212–24.
29. Avrami M. Granulation, phase change, and microstructure kinetics of phase change. III. J Chem Phys. 1941;9:177–84.
30. Johnson WA, Mehl RF. Reaction kinetics in processes of nucleation and growth. Trans Am Inst Min Met Eng. 1939;135: 416–42.
31. Kolmogorov A. On the static theory of metal crystallization. Izv Akad Nauk USSR Ser Fiz. 1937;3:355–9.
32. Farjas J, Roura P. Solid-phase crystallization under continuous heating: kinetic and microstructure scaling laws. J Mat Res. 2008;23:418–26.
33. Criado J, González M, Málek J, Ortega A. The effect of the CO_2 pressure on the thermal decomposition kinetics of calcium carbonate. Thermochim Acta. 1995;254:121–27.
34. Vyazovkin S. Modification of the integral isoconversional method to account for variation in the activation energy. J Comput Chem. 2001;22:178–83.
35. Gallagher PK, Johnson DW. The effects of sample size and heating rate on the kinetics of the thermal decomposition of $CaCO_3$. Thermochimic Acta. 1973;6:67–83.
36. Salvador AR, Garcia Calvo E, Aparicio CB. Effects of sample weight, particle size, purge gas and crystalline structure on the observed kinetic parameters of calcium carbonate decomposition. Thermochim Acta. 1989;143:339–45.
37. Roduit B. Computational aspects of kinetic analysis. Part E: the ICTAC kinetics project-numerical techniques and kinetics of solid state processes. Thermochim Acta. 2000;355:171–80.
38. Málek J. The kinetic-analysis of nonisothermal data. Thermochim Acta. 1992;200:257–69.
39. Budrugeac P. The Kissinger law and the IKP method for evaluating the non-isothermal kinetic parameters. J Therm Anal Calorim. 2007;89:143–51.